ADVANCES IN ATMOSPHERIC SCIENCES, VOL. 31, SEPTEMBER 2014, 1035–1050

Assessment of Future Drought in Southwest China Based on CMIP5 Multimodel Projections

WANG Lin[1,2], CHEN Wen*[1], and ZHOU Wen[3]

[1]*Center for Monsoon System Research, Institute of Atmospheric Physics, Chinese Academy of Sciences, Beijing* 100190
[2]*University of Chinese Academy of Sciences, Beijing* 100049
[3]*Guy Carpenter Asia-Pacific Climate Impact Centre, School of Energy and Environment, City University of Hong Kong, Hong Kong*

(Received 18 November 2013; revised 8 February 2014; accepted 20 February 2014)

ABSTRACT

In the last decade, a series of severe and extensive droughts have swept across Southwest China, resulting in tremendous economic losses, deaths, and disruption to society. Consequently, this study is motivated by the paramount importance of assessing future changes in drought in Southwest China. Precipitation is likely to decrease over most parts of Southwest China around the beginning of the century, followed by widespread precipitation increases; the increase in potential evapotranspiration (PET), due to the joint effects of increased temperature and surface net radiation and decreased relative humidity, will overwhelm the whole region throughout the entire 21st century. In comparative terms, the enhancement of PET will outweigh that of precipitation, particularly under Representative Concentration Pathway (RCP) 8.5, resulting in intensified drought. Generally, the drying tendency will be in the southeast portion, whereas the mountainous region in the northwest will become increasingly wetter owing to abundant precipitation increases. Droughts classified as moderate/severe according to historical standards will become the norm in the 2080s under RCP4.5/RCP8.5. Future drought changes will manifest different characteristics depending on the time scale: the magnitude of change at a time scale of 48 months is nearly twice as great as that at 3 months. Furthermore, we will see that not only will incidences of severe and extreme drought increase dramatically in the future, but extremely wet events will also become more probable.

Key words: drought, Standardized Precipitation Evapotranspiration Index, spatial disaggregation, Southwest China

Citation: Wang, L., W. Chen, and W. Zhou, 2014: Assessment of future drought in Southwest China based on CMIP5 multimodel projections. *Adv. Atmos. Sci.*, **31**(5), 1035–1050, doi: 10.1007/s00376-014-3223-3.

1. Introduction

In recent decades, severe and sustained droughts have frequently hit Southwest China, with the summer of 2006 (Peng et al., 2007), the autumn of 2009 to the spring of 2010 (Huang et al., 2012), and the late summer of 2011 (Sun et al., 2012; Wang et al., 2012) being record-breaking events during the last 50 years. All these events caused devastating and far-reaching consequences to agriculture, water availability, ecosystems (Zhang et al., 2012a; Zhang et al., 2012b), the economy, and society (Ye et al., 2012). Besides the lack of effective precipitation, the complex topography, erosion, deforestation, and poor water management exacerbate the worst drought events in Southwest China (Qiu, 2010). These calamitous droughts in Southwest China have received widespread attention from both the Chinese government and the academic sector.

Increasing research efforts have been dedicated to studying the historical changes and causes of severe droughts in Southwest China. Wang and Chen (2012) investigated the characteristics of drought over Southwest China in the last 100 years and concluded that the emergence of extreme drought in recent years can be attributed to the co-occurrence of precipitation deficits at different time scales. Based on the humidity index, Zhang et al. (2013a) explored the geographic features of the changes in extreme drought frequency from 1960 to 2009 over Southwest China. Moreover, several atmospheric affecting factors related to droughts have been proposed in order to understand the mechanisms leading to drought in Southwest China. For the summer drought of 2006, two potential contributors have been identified: the westward shift and intensification of the western Pacific subtropical high (WPSH) (Li et al., 2009), possibly resulting from above-normal condensation heating in the Bay of Bengal and South China Sea (Peng et al., 2007); and the northward shift of midlatitude westerlies that are unfavorable for the intrusion of cold air. For the prolonged drought from the autumn of 2009 until the spring of 2010, an extremely negative phase of the Arctic Oscillation played an important role

* Corresponding author: CHEN Wen
Email: cw@post.iap.ac.cn

in bringing the track of cold air invasion eastward, leading to weakened convergence of warm moist air from the south and cold dry air from the north (Barriopedro et al., 2012; Huang et al., 2012; Yang et al., 2012). More recently, Zhang et al. (2013b) discussed the possible influence of ENSO Modoki on the autumn drought over Southwest China. Finally, the summer drought in 2011 was possibly induced by the combined effect of weak moisture transport from the Bay of Bengal, a positive geopotential height anomaly, and a more easterly location of the WPSH (Sun et al., 2012; Wang et al., 2012).

However, few studies have focused on the future changes in drought risk in Southwest China under global warming, which is crucial to advance planning for agricultural adaptation, water resource management, human health etc. Under the background of significant climate change (Zhou et al., 2006; Chen et al., 2006; Wei et al., 2011), as well as increased extreme weather events (Zhou et al., 2009; Yuan et al., 2012; Nath et al., 2014) in China in the past decades, several studies have examined future changes in drought in China at a nationwide scale (Xu and Xu, 2012; Chen et al., 2013). Nevertheless, a comprehensive evaluation of future changes in drought in Southwest China has not yet been performed and is the primary motivation for this study. To gain a better insight into the future changes in drought over Southwest China, the downscaling technique of spatial disaggregation is utilized to provide finer-resolution information, and Standardized Precipitation Evapotranspiration Index (SPEI) is used to reveal multiscalar changes in drought.

The paper is structured as follows. The data and methodologies are introduced in sections 2 and 3. The projected spatial and temporal changes in precipitation and potential evapotranspiration (PET) and their relative magnitude are presented in section 4, followed by an assessment of future drought scenarios from the perspective of SPEI in section 5. Finally, section 6 summarizes the conclusions.

2. Data

The monthly precipitation observations used in this study are a gridded dataset that has $0.5^\circ \times 0.5^\circ$ horizontal grids and covers the period from 1961 to 2011, provided by the National Meteorological Information Center of the China Meteorological Administration. This dataset is created based on an interpolation method called thin plate smoothing splines (Hutchinson, 1998a, 1998b), and it is derived from 2474 ground observatories in China that have been subjected to rigorous quality control. In parallel, the gridded observed PET dataset at monthly intervals from 1901 to 2011 is retrieved from the latest version (TS3.2) (Harris et al., 2013) of the Climatic Research Unit (CRU) of the University of East Anglia. The horizontal grid of the PET dataset provided by CRU coincides with that of the precipitation data prepared by the China Meteorological Administration, which facilitates further study without introducing added uncertainties due to the interpolation scheme.

Coupled model data of a historical run that includes all forcings from 1850 to 2005 and two future projection simulations from 2006 to 2099 under two emissions scenarios—namely, Representative Concentration Pathway (RCP) 4.5 (medium mitigation scenario) and RCP8.5 (high emission scenario), as defined in Moss et al. (2010)—are extracted from the World Climate Research Programme (WCRP) Coupled Model Intercomparison Project Phase 5 (CMIP5) (Taylor et al., 2012). Outputs from 23 coupled climate models are employed in this study, as summarized in Table 1. To derive PET and subsequently the drought index, the climate variables from model outputs used in this study are near-surface air temperature including mean, minimum, and maximum, surface pressure, wind speed at 10 m, precipitation, surface downwelling shortwave radiation, surface upwelling shortwave radiation, surface downwelling longwave radiation, surface upwelling longwave radiation, and near-surface relative humidity.

In this study, Southwest China as a study area covers Chongqing, Sichuan, Guizhou, Yunnan, and west of Guangxi, as illustrated in Fig. 1. The period of 1961 to 1990 was recommended by Trewin (2007) and is chosen as the baseline period to perform spatial disaggregation, to calibrate drought indices, and to derive anomalies. Two reasons for the choice of reference period are: (1) high quality of observational data; and (2) avoidance of the massive drought events in recent decades in order to obtain typical conditions. In this study, climatological scenarios are determined by the changes in average climate for 30-year periods centered on the 2020s (2010–39, beginning-of-century), 2050s (2040–69, mid-century), and 2080s (2070–99, end-of-century) relative to the 1961–90 baseline period.

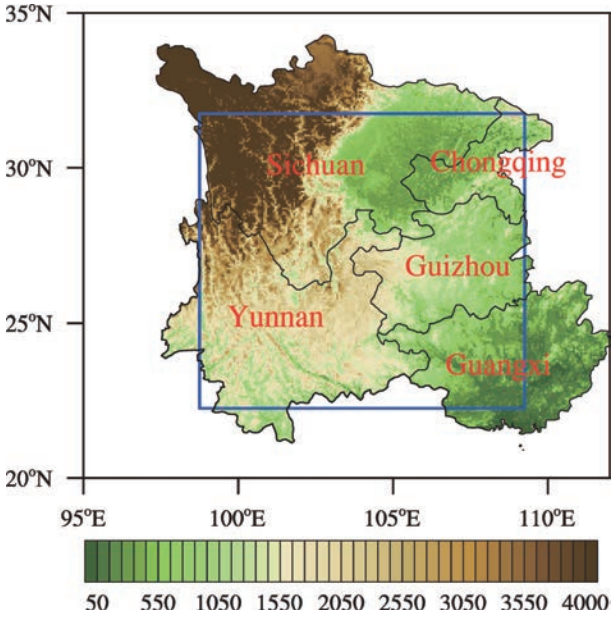

Fig. 1. Study domain showing topography (shading; units: m). The regional mean over Southwest China is obtained by averaging all values within the blue rectangle (22.25°–31.75°N, 98.75°–109.25°E).

Table 1. Summary of 23 climate models from CMIP5 used in this study.

Model	Modeling center	Atmospheric component resolution (Lon × Lat)
ACCESS1-0	Commonwealth Scientific and Industrial Research Organization (CSIRO) and Bureau of Meteorology (BOM), Australia	$1.875^\circ \times 1.25^\circ$
ACCESS1-3	Commonwealth Scientific and Industrial Research Organization (CSIRO) and Bureau of Meteorology (BOM), Australia	$1.875^\circ \times 1.25^\circ$
bcc-csm1-1	Beijing Climate Center, China Meteorological Administration, China	$\sim 2.8^\circ \times 2.8^\circ$
BNU-ESM	College of Global Change and Earth System Science, Beijing Normal University, China	$\sim 2.8^\circ \times 2.8^\circ$
CanESM2	Canadian Centre for Climate Modelling and Analysis, Canada	$\sim 2.8^\circ \times 2.8^\circ$
CESM1-CAM5	Community Earth System Model Contributors, USA	$1.25^\circ \times 0.9^\circ$
CNRM-CM5	Centre National de Recherches Météorologiques/Centre Européen de Recherche et Formation Avancées en Calcul Scientifique, France	$\sim 1.4^\circ \times 1.4^\circ$
CSIRO-Mk-3-6-0	Commonwealth Scientific and Industrial Research Organization in collaboration with the Queensland Climate Change Centre of Excellence, Australia	$1.875^\circ \times 1.875^\circ$
GFDL-CM3	NOAA Geophysical Fluid Dynamics Laboratory, USA	$2.5^\circ \times 2^\circ$
GFDL-ESM2G	NOAA Geophysical Fluid Dynamics Laboratory, USA	$2.5^\circ \times 2^\circ$
GFDL-ESM2M	NOAA Geophysical Fluid Dynamics Laboratory, USA	$2.5^\circ \times 2^\circ$
GISS-E2-H	NASA Goddard Institute for Space Studies, USA	$2.5^\circ \times 2^\circ$
GISS-E2-R	NASA Goddard Institute for Space Studies, USA	$2.5^\circ \times 2^\circ$
HadGEM2-CC	Met Office Hadley Centre (additional HadGEM2-ES realizations contributed by Instituto Nacional de Pesquisas Espaciais), United Kingdom	$1.875^\circ \times 1.25^\circ$
HadGEM2-ES	Met Office Hadley Centre (additional HadGEM2-ES realizations contributed by Instituto Nacional de Pesquisas Espaciais), United Kingdom	$1.875^\circ \times 1.25^\circ$
inmcm4	Institute for Numerical Mathematics, Russia	$2^\circ \times 1.5^\circ$
IPSL-CM5A-LR	Institut Pierre-Simon Laplace, France	$3.75^\circ \times 1.875^\circ$
IPSL-CM5A-MR	Institut Pierre-Simon Laplace, France	$2.5^\circ \times 1.25^\circ$
IPSL-CM5B-LR	Institut Pierre-Simon Laplace, France	$3.75^\circ \times 1.875^\circ$
MIROC5	Atmosphere and Ocean Research Institute (The University of Tokyo), National Institute for Environmental Studies, and Japan Agency for Marine-Earth Science and Technology, Japan	$\sim 1.4^\circ \times 1.4^\circ$
MIROC-ESM	Japan Agency for Marine-Earth Science and Technology, Atmosphere and Ocean Research Institute (The University of Tokyo), and National Institute for Environmental Studies, Japan	$\sim 2.8^\circ \times 2.8^\circ$
MIROC-ESM-CHEM	Japan Agency for Marine-Earth Science and Technology, Atmosphere and Ocean Research Institute (The University of Tokyo), and National Institute for Environmental Studies, Japan	$\sim 2.8^\circ \times 2.8^\circ$
MRI-CGCM3	Meteorological Research Institute, Japan	$1.125^\circ \times 1.125^\circ$

3. Methodologies

3.1. *Spatial disaggregation as a downscaling technique*

Spatial disaggregation used as a downscaling technique was originally developed by Wood et al. (2002, 2004) to improve streamflow forecasts and was later adopted in many climate change impact studies (e.g., Hayhoe et al., 2008; Wang and Chen, 2013). Spatial disaggregation uses GCM precipitation as a predictor, making it possible to capture the complexity of physical processes in a way that cannot be achieved using only larger-scale circulation indicators (Maurer and Hidalgo, 2008). In addition, Widmann et al. (2003) suggested that using local predictors such as precipitation yielded a performance comparable with other downscaling methods. In this study, the monthly GCM precipitation and PET for all climate models and the two future emissions scenarios (RCP4.5 and RCP8.5) are downscaled to a resolution of 0.5°, identical with that of observations.

Figure 2 displays the detailed process of spatial disaggregation of the modeled precipitation from IPSL-CM5A-LR in May 1986. First, the spatial climatology pattern for observed precipitation in May is derived (Fig. 2a). Second, the resulting pattern obtained in the preceding step is aggregated to a GCM-specific scale (Fig. 2b). Third, the factor values (Fig. 2d) as ratios of the GCM (Fig. 2c) to the coarsened climatology of observations (Fig. 2b) are calculated. Fourth, the coarse-scale factor values (Fig. 2d) are translated via bilinear interpolation to the targeted downscaled resolution (Fig. 2e), $0.5^\circ \times 0.5^\circ$. And finally, the interpolated factor map (Fig. 2e) is multiplied by the original observed climatology (Fig. 2a) to generate the finer-scale spatial pattern of GCM outputs (Fig. 2f).

3.2. *SPEI as a drought index*

SPEI, recently proposed by Vicente-Serrano et al. (2009, 2010), combines the multiscalar nature and simplicity of the Standardized Precipitation Index (SPI) calculation (McKee et al., 1993, 1995) and the sensitivity of the Palmer Drought Severity Index (PDSI) (Palmer, 1965; Wells et al., 2004) to change in evaporative demand caused by temperature, radiation and wind fluctuations. Besides the inclusion of the role of evapotranspiration in the calculation procedure, the main advantage of SPEI lies in its capability to identify different types of drought (Vicente-Serrano et al., 2011): me-

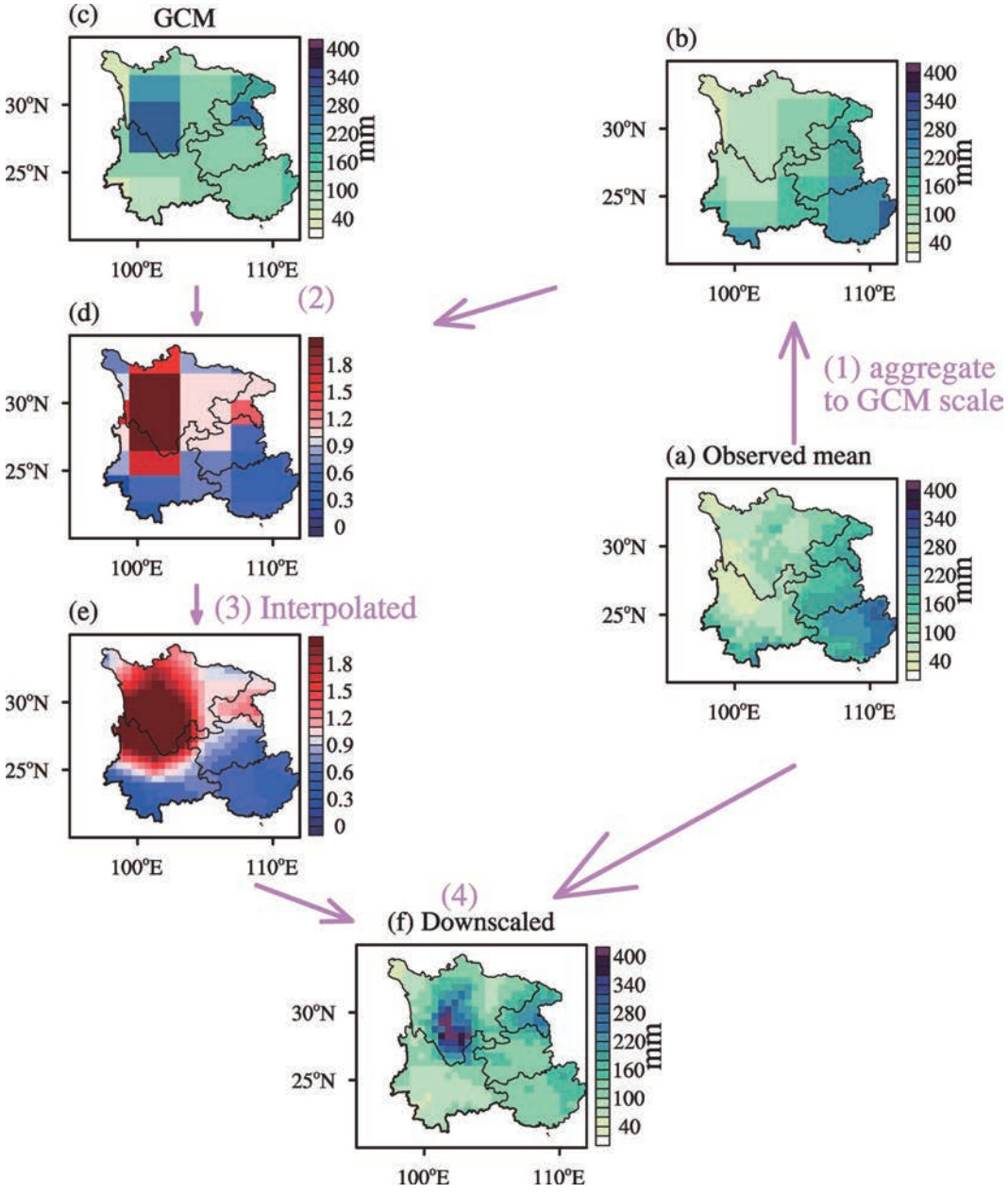

Fig. 2. Schematic illustration of the spatial disaggregation process. The downscaled precipitation field is constructed from IPSL-CM5A-LR outputs for May 1986.

teorological, agricultural and hydrological drought (Wilhite, 2006). As reported by McKee et al. (1995), Byun and Wilhite (1999) and Hayes et al. (1999), it is commonly accepted that drought is a multiscalar phenomenon, highlighting the utility of multiscalar drought index—SPEI as an indicator to capture drought impact on different usable water resources. Moreover, the ability of SPEI to reproduce drought conditions has been validated in many works, e.g., Vicente-Serrano et al. (2012) and McEvoy et al. (2012). In particular, Wang and Chen (2014) have substantiated the applicability of SPEI and its strength over PDSI and SPI in China. Consequently, SPEI is exploited in this study to measure the drought severity at multiple time scales. Table 2 shows the classification of drought according to SPEI values.

Table 2. Classification of drought and corresponding probability according to SPEI values.

SPEI values	Drought category		Probability (%)
$\geqslant 2.0$	extreme wet		2.3
1.5 to 1.99	severe wet		4.4
1 to 1.49	moderate wet		9.2
0 to 0.99	mild wet	near-normal	34.1
0 to -0.99	mild drought	near-normal	34.1
-1 to -1.49	moderate drought		9.2
-1.5 to -1.99	severe drought		4.4
$\leqslant -2.0$	extreme drought		2.3

A brief description of the main steps and specific settings to derive SPEI is provided here. (1) The monthly PET is first computed based on Penman–Monteith parameterization discussed in section 3.3. (2) The difference between precipitation (P) and PET for the month i is calculated:

$$D_i = P_i - \mathrm{PET}_i \ . \tag{1}$$

(3) The calculated D_i values are aggregated at different time scales:

$$D_n^k = \sum_{i=0}^{k-1} (P_{n-i} - \mathrm{PET}_{n-i}) \ , \quad n \geqslant k \ , \tag{2}$$

where k (months) is the time scale of the aggregation and n is the calculation month. (4) The data series of D are fitted to the Log-logistic distribution and then normalized to obtain SPEI values. The Log-logistic distribution is given by:

$$f(x) = \frac{\beta}{\alpha}\left(\frac{x-\gamma}{\alpha}\right)^{\beta-1}\left[1+\left(\frac{x-\gamma}{\alpha}\right)^{\beta}\right]^{-2} \ , \tag{3}$$

where α, β, γ are scale, shape and origin parameters, respectively. The complete calculation procedure of SPEI is available in Vicente-Serrano et al. (2009). In this study, SPEI series at the time scales of 3, 6, 12, 24, and 48 months, which are typical time scales for precipitation deficits to affect the five types of usable water, as recommended by McKee et al. (1993), are calculated and the calibration period chosen is from 1961 to 1990.

3.3. *Potential evapotranspiration estimate*

The two most prominent approaches with extensive applications to estimate PET are the Thornthwaite (Thornthwaite, 1948) and Penman–Monteith (Allen et al., 1994) schemes. The Thornthwaite method is the simplest way to parameterize PET because of its low requirement for input data: only monthly mean temperature and the latitude of the location are necessary. However, a major deficiency of the Thornthwaite method is its overestimation of PET, especially in the tropics, which is closely associated with the exclusion of cloud cover and vapor pressure deficit (Hobbins et al., 2008; van der Schrier et al., 2011). In future climate scenarios, the Thornthwaite algorithm may overestimate the potential evaporation and predict an unrealistic increase in drought frequency, as suggested by Burke et al. (2006).

A more realistic method than the Thornthwaite equation for quantifying PET, and one that is recommended by the Food and Agriculture Organization (FAO) of the United Nations, is the Penman–Monteith approach (Allen et al., 1994), which accounts for the combined effects of temperature, radiation, humidity, and wind speed. By definition, the Penman–Monteith PET calculates the rate of evapotranspiration from a hypothetical reference crop with an assumed crop height of 0.12 m, an albedo of 0.23, and a fixed surface resistance of 70 s m^{-1}. The Penman–Monteith PET is formulated as:

$$\mathrm{PET} = \frac{0.408\Delta(R_\mathrm{n} - G) + \gamma\dfrac{900}{T+273}U_2(e_\mathrm{a} - e_\mathrm{d})}{\Delta + \gamma(1 + 0.34U_2)} \ , \tag{4}$$

where Δ is the slope of the saturation vapor pressure function of temperature in kPa $^\circ$C^{-1}, R_n is the net radiation in MJ m^{-2} d^{-1}, G is soil heat flux in MJ m^{-2} d^{-1}, γ is the psychrometric constant in kPa $^\circ$C^{-1}, T is the mean surface temperature in $^\circ$C, U_2 is the wind speed at 2 m above the surface in m s^{-1}, and e_a and e_d are the saturation and actual vapor pressure in kPa, respectively. In this study, the Penman–Monteith parameterization is employed to derive PET.

4. Projected changes in precipitation and PET

Though the ultimate objective of this study is to assess projected changes in the drought index, we will first outline how precipitation and PET—two key climatic variables determining the wet/dry state—will change temporally and spatially in the future so that we can better illuminate the driving processes underlying changes in drought. Hereafter, climatological changes in precipitation, PET, and SPEI from the reference period (1961–90) to the projection periods (2010–39, 2040–69, or 2070–99) are denoted as ΔP, ΔPET, and ΔSPEI, respectively.

4.1. *Precipitation*

Presented in Fig. 3 is the geographic distribution of climatological change in precipitation, in terms of multimodel ensemble means in the 2020s, 2050s, and 2080s compared to the baseline period (1961–90). In addition, the uncertainties of the projection are examined by counting the number of models with a change of the same sign as the multimodel ensemble mean. The threshold chosen in this study is 70% (16 out of 23).

For the beginning-of-century period, precipitation appears to decrease over most parts of Southwest China and there is good consensus among the various GCMs. In particular, the maximum decreases are located on the border between Yunnan, Sichuan, and Guizhou, ranging from approximately 5% to 7%. However, it is probable that more precipitation will fall in the northwest part of the study domain. The dominant feature in the mid- and end-of-century periods is an overall increase in precipitation across Southwest China, with a remarkable change of 10% compared to 1961–90 climatology in the mountainous regions. In contrast to the beginning-of-century period, the precipitation increase over most areas suggested by the multimodel ensemble mean is subject to considerable uncertainty. However, much stronger agreement over the northwest is notable and persists throughout the 21st century. The spatial patterns of precipitation responses are similar between the RCP4.5 and RCP8.5 scenarios, with the correlation coefficients being 0.97, 0.94, and 0.95 for the three future time periods, indicating a limited effect of greenhouse gas (GHG) concentrations on the pattern of future changes in precipitation (Figs. 3c, f, and i). To illuminate the atmospheric factors causing the projected pattern of precipitation change, Fig. S1 in the supplementary information shows the future change in water vapor flux and associated divergence over East Asia. The precipitation

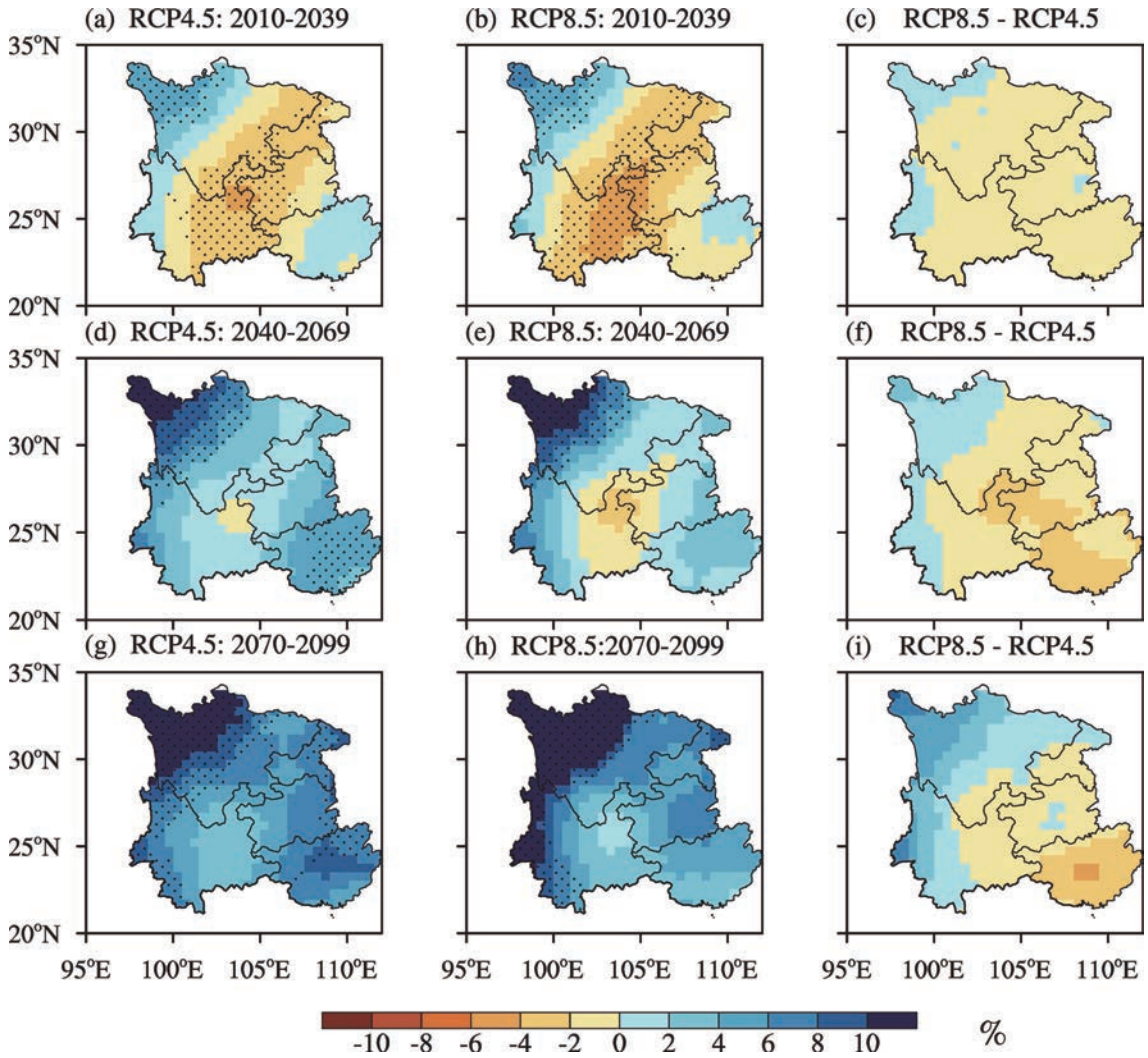

Fig. 3. Spatial distribution of the percentage change in climatological precipitation (%) from the reference period (1961–90) to 2010–39 (Top row), 2040–69 (middle row), and 2070–99 (bottom row) under RCP4.5 (left column) and RCP8.5 (middle column). The difference between precipitation change under RCP8.5 and RCP4.5 is shown in right column. The stippling in (a, b, d, e, g, h) indicates where at least 70% (16 out of 23) of all participant GCMs agree on the sign of the mean change in a given grid cell.

increase over Southwest China after the mid-century period results from the intensified water vapor transport from the Bay of Bengal and enhanced moisture convergence. In the beginning-of-century period, however, the center of Southwest China is dominated by anomalous moisture divergence, which favors a decrease in precipitation.

Figures 4a and b display changes in annual mean precipitation anomalies averaged over Southwest China under RCP4.5 and RCP8.5 from 1961 to 2099 compared to the 1961–90 averages. Uncertainty, as depicted by the blue shading, is quantified by the interquartile range across the CMIP5 ensemble—a more robust measure than the minimum to maximum range, which is vulnerable to outliers. For past variation in precipitation, although the amplitudes given by the multimodel ensemble mean are smaller than those of the observations, the decreasing trend in observed precipitation is well captured by the GCMs. Compared with the historical period, however, from the beginning of the 21st century both the RCP4.5 and RCP8.5 scenarios demonstrate an increasing trend in precipitation until the 2070s. After this time, the regional mean precipitation continues to increase under RCP8.5, while that under RCP4.5 is projected to stabilize at around 10 mm month^{-1}. The spread of the GCM ensemble is enlarged slightly over time, since the average interquartile ranges for 1961–90, 2010–39, 2040–69, and 2070–99 under RCP4.5 are 13.5, 14.8, 18.2, and 21.4 mm, respectively.

4.2. *PET*

Future changes in PET—another important determinant of drought besides precipitation—are highlighted in Fig. 5. Widespread increases in PET cover the whole region throughout the 21st century, with a relatively pronounced increase projected over northern and eastern parts of Southwest China. The different emissions scenarios do not lead to dramatically

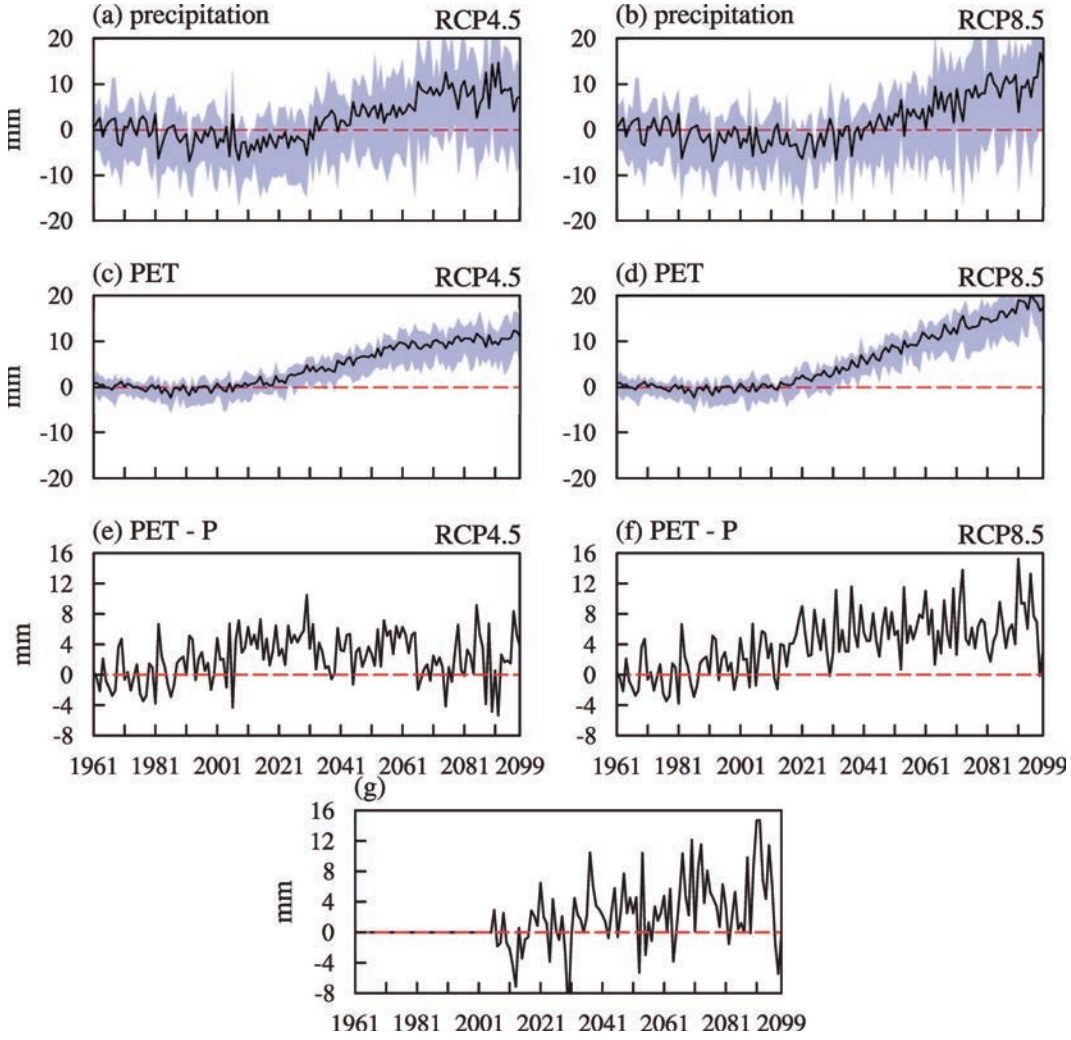

Fig. 4. Anomalies of (a, b) annual mean precipitation, (c, d) PET, and (e, f) PET $-$ *P* under RCP4.5 and RCP8.5 averaged over Southwest China during 1961–2099 relative to the 1961–90 climatology. The difference between PET $-$ *P* under RCP8.5 and RCP4.5 is shown in (g). The black line and blue shading denote the ensemble mean and interquartile range across all GCMs, respectively.

different PET responses in the beginning-of-century period (Fig. 5c). The discrepancies between the PET changes under the two scenarios, however, become more and more noticeable after the mid-century period, especially at the end of the century (Figs. 5f and i). The difference between the spatial patterns of the change in PET under RCP4.5 and RCP8.5 for the 2080s, quantified by the root-mean-square difference, is 6 mm, compared to 0.3 mm for the 2020s. Before 2050, as shown in Figs. 4c and d, the increase in PET under RCP4.5 and RCP8.5 exhibits roughly identical behavior. However, the magnitude of the increase in PET under RCP8.5 is nearly twice that under RCP4.5 at the end of the century: 20 mm versus 10 mm in terms of the multimodel ensemble mean. It is evident that, in contrast to considerable uncertainty in projected changes in precipitation (Figs. 4a and b), nearly all GCMs exhibit a consistent increasing signal in PET.

As indicated by Fig. 6, the future increase in PET can be ascribed to the joint effect of an increase in surface temperature and net radiation and a decrease in relative humidity. Interannual variability in surface net radiation, temperature, relative humidity, and wind speed are explored in Fig. 6 to illustrate the driving processes behind the changes in PET: (1) As illustrated in Figs. 6a and b, a reduction of net radiation of about 0.9% per decade is found from 1961 to 2010, successfully reproducing the observed trend (Ren et al., 2005), followed by a strong positive trend after 2010 that extends to the end of the 21st century under both emissions scenarios, suggesting an enhancement of PET and thereby an exacerbation of drought. (2) On the one hand, the regional mean temperature is expected to increase by 1.66°C and 1.88°C until 2040 under RCP4.5 and RCP8.5, respectively. On the other hand, by the end of this century, the magnitude of surface warming over Southwest China more than doubles under RCP8.5 compared to RCP4.5, resembling the outcomes from a projection of national average temperature (Xu and Xu, 2012). (3) There has been an overall decreasing trend in relative humidity of $-0.14\%\ (10\ \mathrm{yr})^{-1}$ over the past half century. Moreover, this decrease continues throughout the 21st century. By

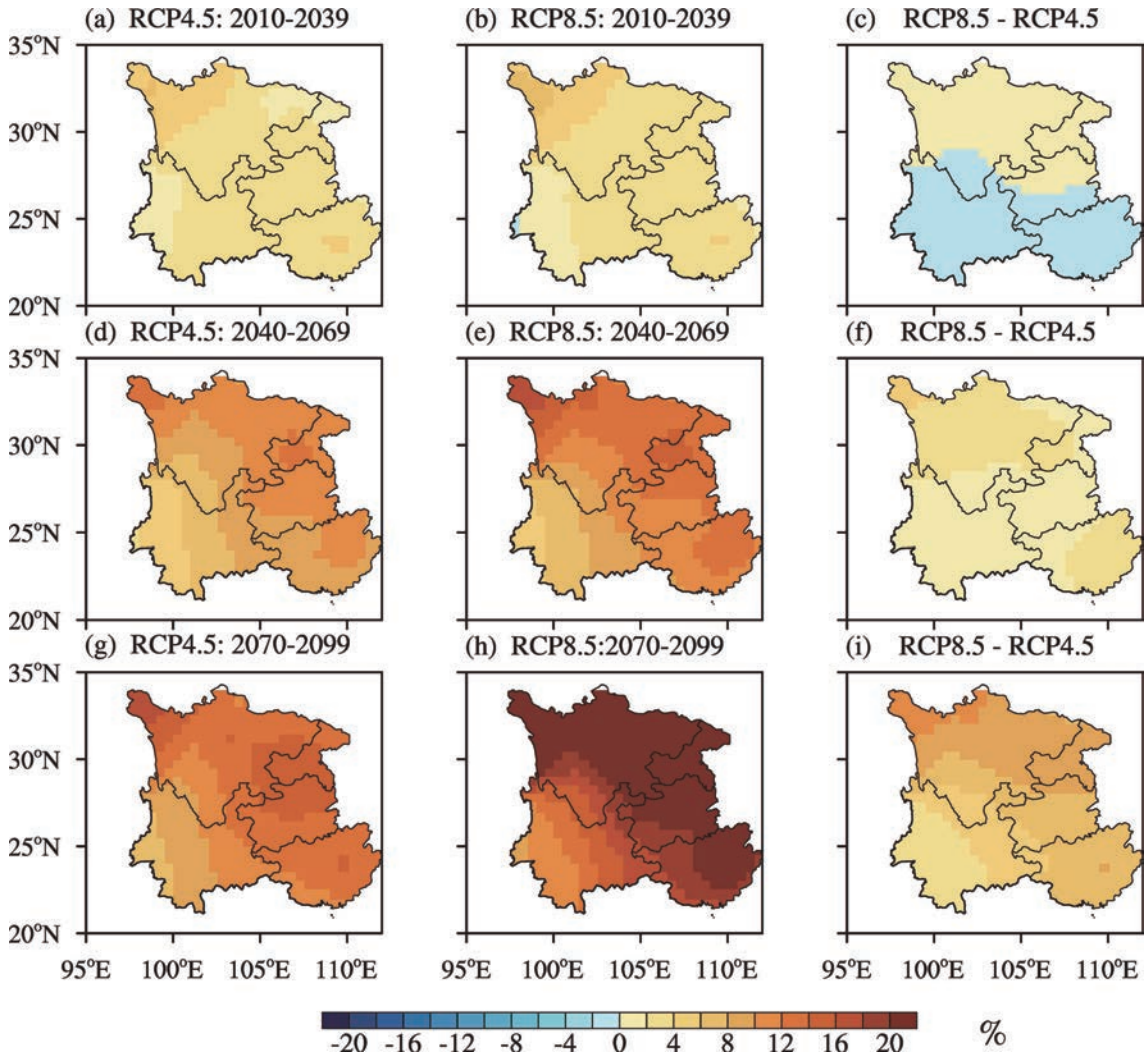

Fig. 5. The same as Fig. 3 but for potential evapotranspiration. The stippling shown in Fig. 3 to indicating how robust these changes are is omitted here due to almost all GCMs agreeing on the sign of the mean change (positive).

2099, the decrease in annual relative humidity is up to 4% in the GCMs under RCP8.5— double that under RCP4.5. (4) It is noticeable that the change in wind speed is commonly confined within 0–0.1 m s^{-1} in the present century, so the influence of changing wind speed on PET can be totally neglected compared to the other three components. In short, projected higher temperatures and net radiation and lower relative humidity collectively intensify PET and thereby aggravate drought severity in the future. Among all potential driving factors, temperature increase plays the dominant role in future enhancement of PET. To substantiate this, we recalculate the projected PET by removing the temperature trend and fluctuation and find that the significant PET increase to a large degree disappears (Fig. S2 in the supplementary information).

4.3. *PET minus precipitation*

Since SPEI is constructed by using the difference between precipitation and PET, and precipitation and PET will both increase in the future as analyzed above, it is necessary to evaluate whether the net change —in other words, PET minus precipitation —will increase or decrease in the future. As shown in Fig. 7, overall, a PET $-$ P increase appears in the southeast part of the study domain accompanied by a remarkable decrease over the northwest. Consequently, the mitigating effect of the precipitation increase over the southeast will be completely overridden by the strengthened PET, while the mountainous region will become wetter and wetter toward the end of this century as a consequence of a notable precipitation increase, as indicated by Fig. 3. Although the direction of change in climatological precipitation is inconclusive due to a lack of agreement between various GCMs, the majority of models reach a consensus that the increasing rate of PET exceeds that of precipitation across Southwest China, excluding the northwest, which will inevitably aggravate water resource scarcity. In the period 2010–39, the increase in PET $-$ P is induced by precipitation deficits as well as an increase in evaporative demand, as shown in Figs. 3 and 5; however, during the remaining time, it is intensified PET that is responsible for the increase in PET $-$ P. In addition, under RCP4.5 the

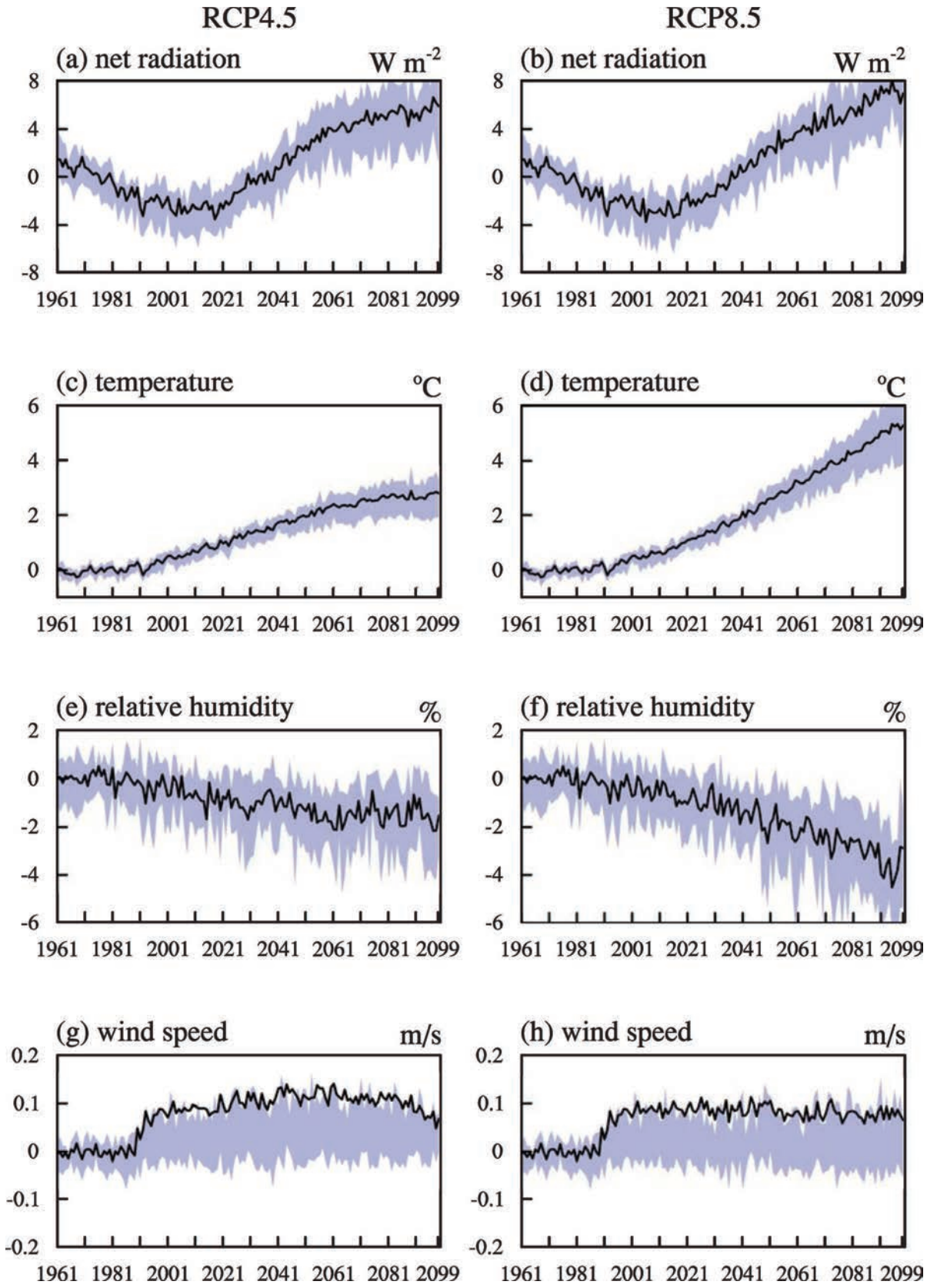

Fig. 6. Anomalies of (a, b) annual mean surface net radiation (units: W m^{-2}), (c, d) temperature (units: °C), (e, f) relative humidity (units: %), and (g, h) wind speed (units: m s^{-1}) under RCP4.5 and RCP8.5 averaged over Southwest China during 1961–2099 relative to the 1961–90 average. The black line and blue shading denote the ensemble mean and interquartile range across all GCMs, respectively.

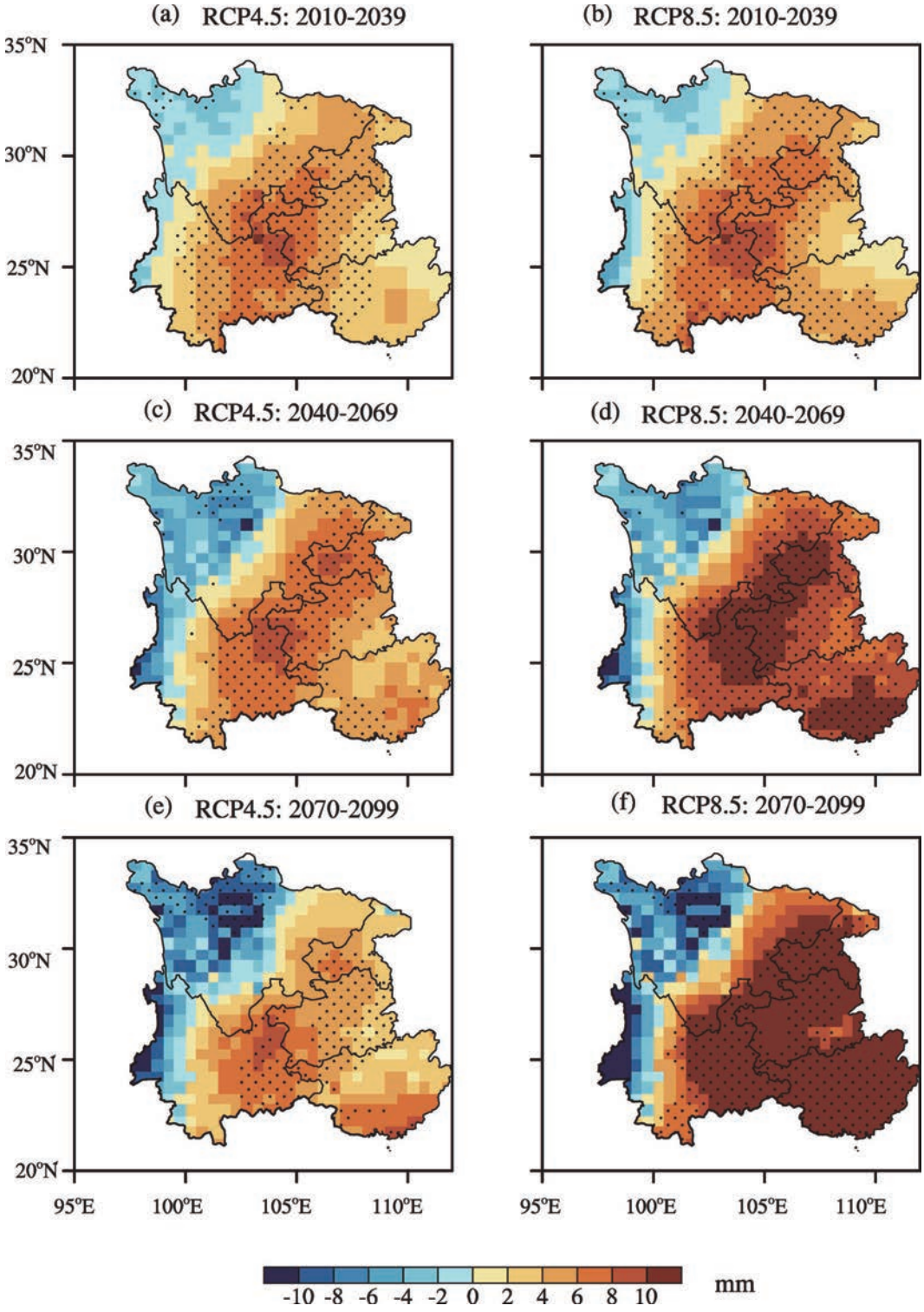

Fig. 7. The same as Fig. 3 but for the differences between PET and precipitation (units: mm month^{-1}).

area with high uncertainty becomes larger and larger toward the end of the 21st century, possibly as a result of the comparable changes in the magnitude of precipitation and PET. Given the larger radiative forcing in the RCP8.5 simulation, however, a significant temperature response is expected and accordingly PET increases more than precipitation increases, so the uncertainty is remarkably damped under RCP8.5. In short, precipitation and PET both demonstrate a persistent upward trend after 2010; in relative terms, it is noteworthy that PET increases faster than precipitation, markedly so under RCP8.5. Finally, it is necessary to stress that the projected pattern of the changes in PET $-$ P over Southwest China results from a physical mechanism rather than noise, since it affects the whole of eastern and southern China (see Fig. S3

in the supplementary information).

5. Projected changes in drought

Figures 8 and 9 show the multimodel ensemble differences in climatological SPEI between the scenario and baseline period at the time scales of 3 months and 48 months, respectively. The multimodel ensemble predicts a drying tendency over Yunnan, Guizhou, Guangxi, Chongqing, and east of Sichuan for both short- and long-term drought. On the other hand, the increase in SPEI is the dominant feature over the northwest portion of the domain, in accordance with the spatial pattern of responses in PET $-$ P, as revealed in Fig. 7. Considering the time scale of 3 months, the magnitudes

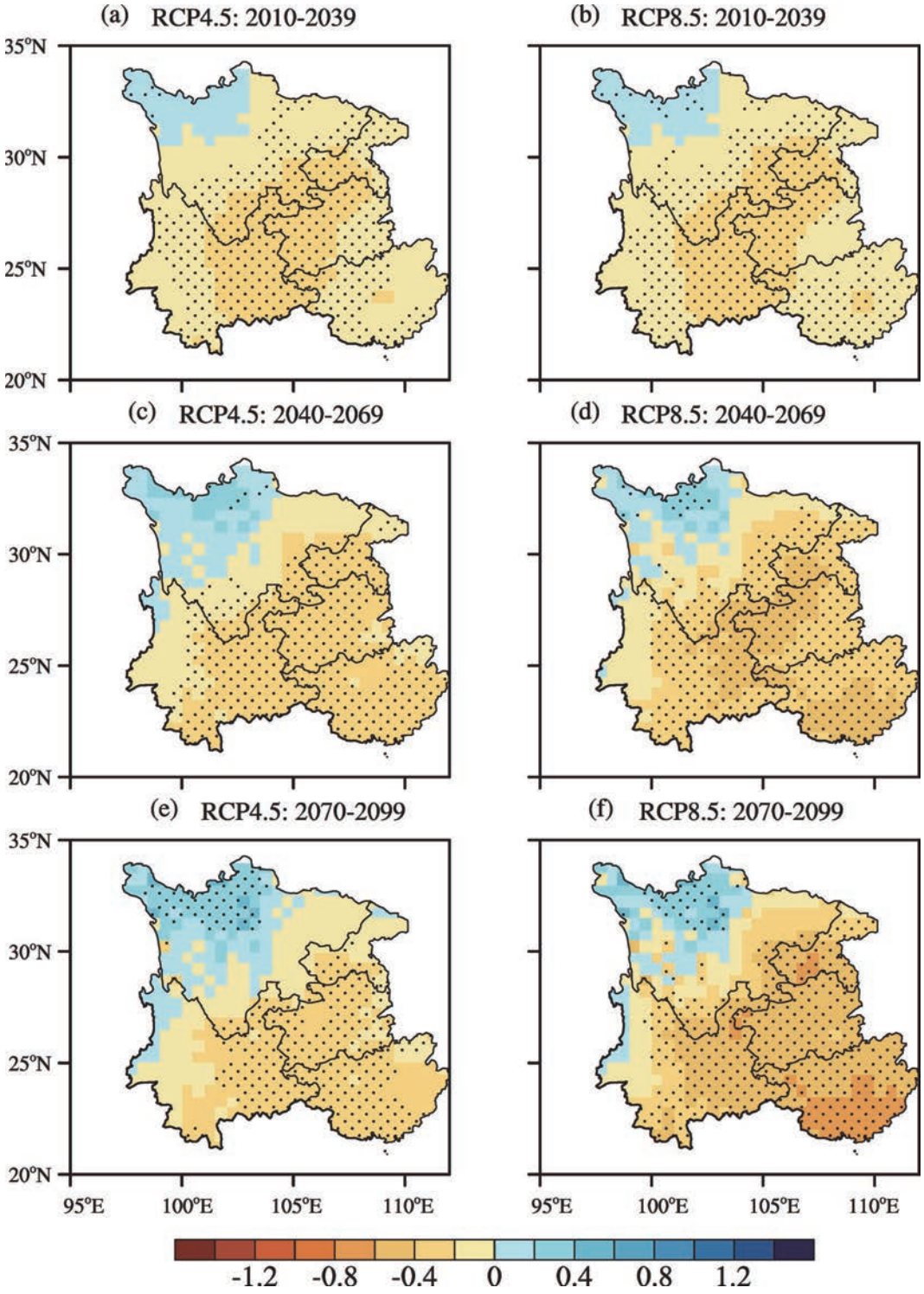

Fig. 8. The same as Fig. 3 but for SPEI at the time scale of 3 months.

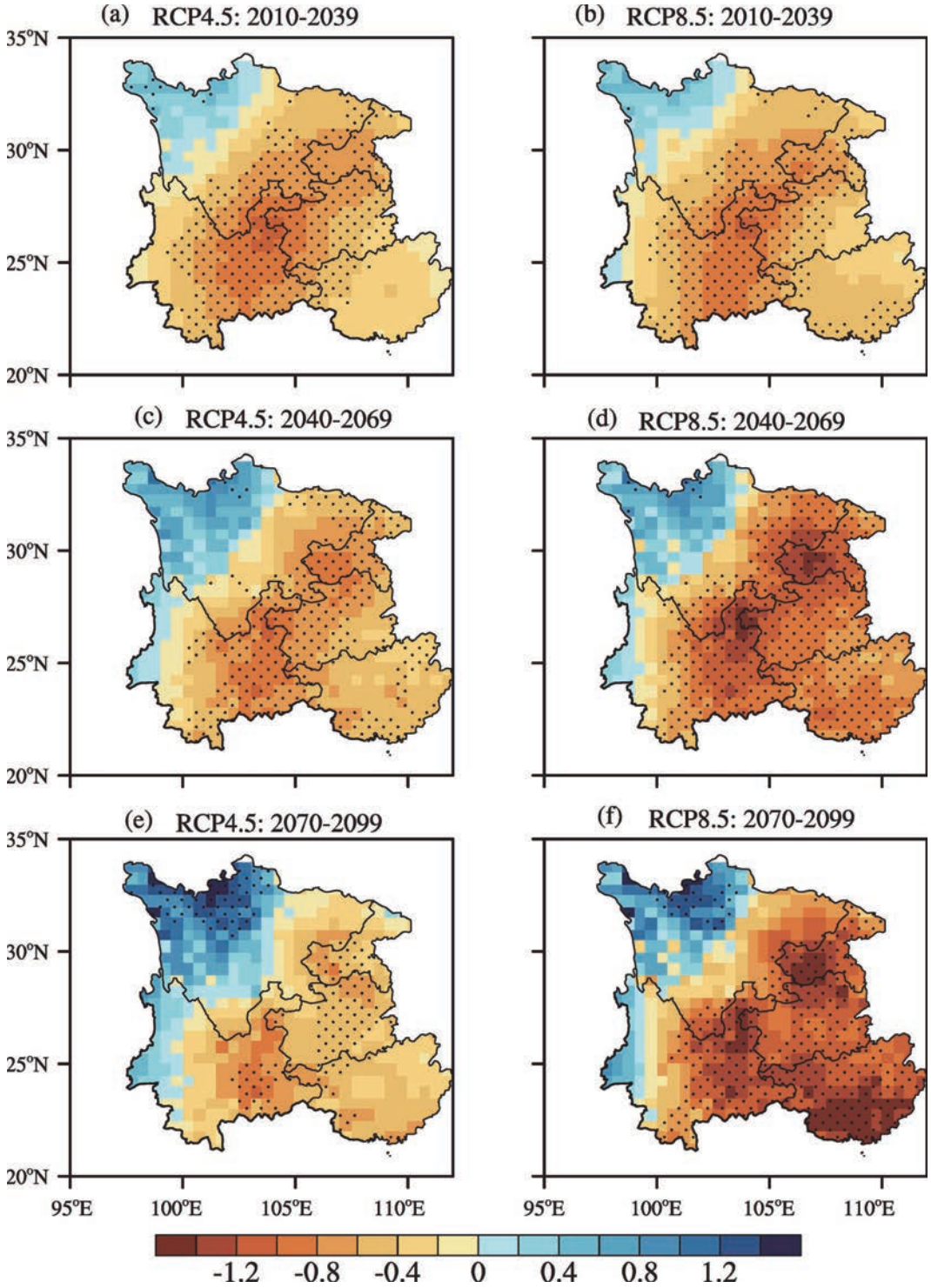

Fig. 9. The same as Fig. 8 but for SPEI at the time scale of 48 months.

and spatial pattern of the change in SPEI are generally comparable over the three future time periods for either RCP4.5 or RCP8.5, ranging from a minimum of −0.4 to a maximum of 0.4. In addition, the respective changes in climatological SPEI under RCP4.5 and RCP8.5 exhibit a consistent spatial pattern and magnitude for any future time period, indicating a negligible effect of emissions scenarios on the projected change in short-term drought. If we inspect the projected change for long-term drought, however, a vastly different story is presented. Under both emissions scenarios, the long-term drought threat (48 months) over the northwest portion is expected to be ameliorated gradually throughout the century due to the remarkable precipitation increase as shown in Fig. 3. However, over the southeast portion, RCP4.5 and

RCP8.5 show different characteristics. Under RCP4.5, the most drying is observed in the beginning-of-century period, with peak values of about −1 in terms of ΔSPEI. Despite the fact that the climatological drought after 2040 is more serious than that in the baseline period, it becomes moderate compared with that in the beginning-of-century period because the grid cells where ΔSPEI increases in the 2080s relative to the 2020s account for 70% of all grids. A substantial decrease of more than 1.5 in SPEI is projected after the mid-century period under RCP8.5 over the southeast, with a high level of model consistency. A comparison of Fig. 9 with Fig. 8 shows that it is at the longer time scales that the magnitude of future changes in SPEI is more significant, which can be interpreted as a consequence of the cumulative effect of drought and SPEI. In the case of longer time scales, the pattern will reinforce due to more frequency of months following the same pattern; the opposite is true for shorter time scales, in which different patterns show up among consecutive months. However, it should also be noted that the time scale can influence only the magnitude of the response, not the sign.

The greatest concern is the projected change in extreme drought events, which are of the same magnitude as the worst droughts in the history of Southwest China. Figure 10 shows the probability distributions of SPEI in the three future time periods at time scales of 6 and 48 months under RCP4.5 and RCP8.5. At any time scale, SPEI during the reference period is standard normally distributed, in line with the mathematical principle of the SPEI procedure. At the time scale of 6 months under RCP4.5, as shown in Fig. 10a, there is no visible change in the mean, but the probability distribution becomes slightly broader with time, and the peak probability decreases accordingly from 17.7% for the baseline period to 14% for the period 2070–99, implying increased variability. Under RCP8.5 at the time scale of 6 months, however, not only is the probability distribution flattened continuously toward the end of this century, but its mean also shifts to the left to some extent, and the central value corresponding to the peak probability decreases by 0.5. In addition, the time spent in dry conditions (SPEI < 0) is about 7.7%–14.9% and 14.6%–19.4%, depending on the period in question, more than that in wet conditions (SPEI > 0) under RCP4.5 and RCP8.5, respectively. Comparing the second row with the first in Fig. 10, it is evident that the probability distribution of

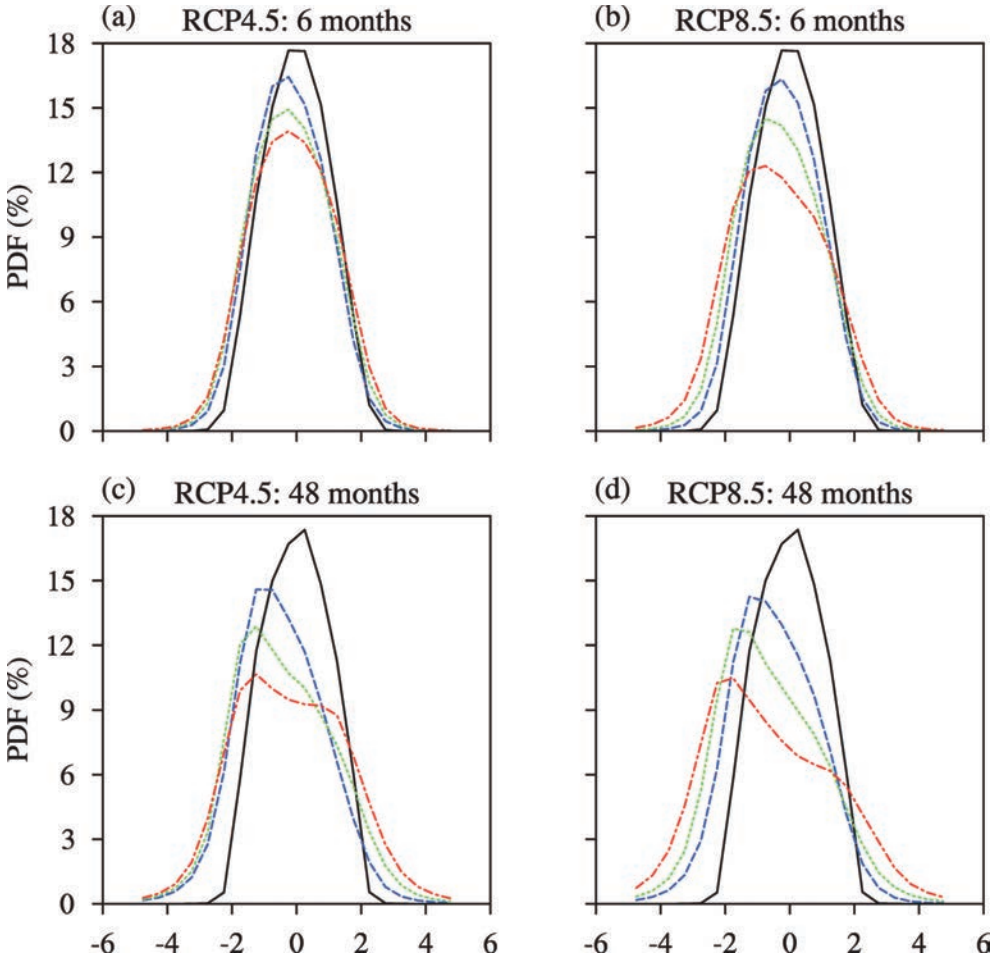

Fig. 10. Probability distributions of SPEI at the time scales of 6 and 48 months under RCP4.5 (1st column) and RCP8.5 (2nd column). The black, blue, green, and red lines represent the probability distributions during the reference period (1961–90), 2010–39, 2040–69, and 2070–99, respectively. See text for details on the procedure of constructing the probability distribution.

SPEI in either the mean value or variance at the time scale of 48 months will change more drastically than that at 6 months. Details of the probability change of SPEI at the time scale of 48 months are as follows. For the end-of-century period under RCP4.5, the central value of the probability distribution moves from about 0.0 to the bin centered at -1.25, with the peak frequency dropping from 17.7% to 10.6%, indicating that drought classified as moderate by historical standards will become the norm in the 2080s. Due to the shift in the mean, the frequency of extreme drought events (SPEI < -2) is expected to increase to 11.2%–14.5%, depending on the future period considered. It is noteworthy that the risk of extreme drought tends to remain stable as time goes on under RCP4.5, in agreement with the left panel of Fig. 9. Furthermore, though the frequency of dry events will likely increase in the future, the incidence of extreme wet events will rise rather than decrease, because the probability of SPEI being greater than 2.5, almost absent in the reference period, will grow remarkably to 1.4% (beginning-of-century) and 5.7% (end-of-century). In addition, the frequency of extreme wet events shows a steady increase from the beginning- to end-of-century period, in contrast to that of extreme dry events staying at a constant level. Figure 10d shows that the probability distribution of SPEI under RCP8.5 in the beginning-of-century period greatly resembles that under RCP4.5. However, the probability distributions under RCP4.5 and RCP8.5 begin to diverge after the mid-century period. In the end-of-century period, the probability distribution of SPEI shifts more than one and a half standard deviations, peaking at -1.75 with a probability of 10.5%, so drought that is severe according to current climate criteria will become the new norm in the 2080s. Moreover, the chance of extreme events in the form of catastrophic drought (SPEI < -2.5) and vigorous rainfall (SPEI > 2.5) will rise rapidly in the future, from 6.6% in 2010–39 to 22.8% in 2070–99. It can be concluded that the climate in Southwest China will become more extreme in the future.

6. Conclusions

During the last decade, Southwest China has experienced three mega-droughts, which occurred in the summer of 2006, the autumn of 2009 to the spring of 2010, and the late summer of 2011, all of which caused considerable losses including crop failure, lack of drinking water, ecosystem destruction, health problems, and even deaths. Accordingly, much effort has been dedicated to surveying (1) the historical variation in dry/wet conditions over Southwest China in the past 50 or 100 years and (2) the atmospheric circulation mechanism responsible for causing droughts. However, few studies have explored the upcoming change in drought risk in Southwest China, knowledge of which will be helpful in planning for agricultural adaptation strategies, advanced water management, and human health, which were the primary motivations for this study.

In the beginning-of-century period, projected changes in precipitation are rather mixed, with a reliable decrease in the southeastern portion and an increase over the mountainous region, which expands into the whole study domain in the following decades. The widespread increase in PET, linked to increased temperature and surface net radiation and decreased relative humidity, dominates the whole domain throughout the present century. Although the overall trends in precipitation and PET are both upward, the increasing rate of PET exceeds that of precipitation, implying that the possible mitigation effect of increased precipitation may be completely consumed by enhanced evaporation. In addition, the GHG forcing scenario has no substantial impact on the projected change in precipitation over the whole period, and its impact on divergent PET responses under RCP4.5 and RCP8.5 appears after the mid-century period.

For future drought change quantified by SPEI, increasing PET closely associated with surface warming is expected to produce more droughts in most of Southwest China. Even with increased PET, however, the mountainous region in the northwest appears to become wetter and wetter, owing to abundant precipitation increases, which effectively suppress the strengthened evaporation. Furthermore, future drought scenarios depend on the time scale considered: the magnitude of change in SPEI at the time scale of 48 months is nearly twice as great as that at 3 months. The drying/wetting tendency at longer time scales is remarkably stronger than that at shorter time scales. It should also be noted that the time scale can influence the magnitude of the response only, not the sign. Dissecting the projected change in the probability distribution leads to the conclusion that not only will incidences of climatological and extreme drought increase dramatically in the future, but extreme wet events will also become more probable due to increased variability, indicating that extreme events including droughts and floods will become more common in Southwest China.

Acknowledgements. We thank the two anonymous reviewers for their constructive suggestions and comments, which led to a significant improvement in the paper. This work was supported by the National Natural Science Foundation of China (Grant Nos. 41230527, 41175079, and 41025017) and the Jiangsu Collaborative Innovation Center for Climate Change.

Electronic supplementary material: Supplementary material is available in the online version of this article at http://dx.doi.org/10.1007/s00376-014-3223-3.

REFERENCES

Allen, R. G., M. Smith, A. Pereira, and L. S. Perrier, 1994: An update for the calculation of reference evapotranspiration. *ICID Bull.*, **43**(2), 1–34.

Barriopedro, D., C. M. Gouveia, R. M. Trigo, and L. Wang, 2012: The 2009/10 drought in China: Possible causes and impacts on vegetation. *J. Hydrometeor.*, **13**, 1251–1267.

Burke, E. J., S. J. Brown, and N. Christidis, 2006: Modeling the recent evolution of global drought and projections for the

twenty-first century with the Hadley Centre climate model. *J. Hydrometeor.*, **7**, 1113–1125.

Byun, H.-R., and D. A. Wilhite, 1999: Objective quantification of drought severity and duration. *J. Climate*, **12**, 2747–2756.

Chen, H. P., J. Q. Sun, and X. L. Chen, 2013: Future changes of drought and flood events in China under global warming scenario. *Atmos. Oceanic Sci. Lett.*, **6**(1), 8–13.

Chen, W., L. H. Kang, and D. Wang, 2006: The coupling relationship between summer rainfall in China and global sea surface temperature. *Climatic and Environmental Research*, **11**(3), 259–269. (in Chinese)

Harris, I., P. D. Jones, T. J. Osborn, and D. H. Lister, 2013: Updated high-resolution grids of monthly climatic observations-the CRU TS3.10 dataset. *Int. J. Climatol.*, doi: 10.1002/joc.3711.

Hayes, M. J., M. D. Svoboda, D. A. Wilhite, and O. V. Vanyarkho, 1999: Monitoring the 1996 drought using the Standardized Precipitation Index. *Bull. Amer. Meteor. Soc.*, **80**, 429–438.

Hayhoe, K., and Coauthors, 2008: Regional climate change projections for the Northeast USA. *Mitig. Adapt. Strat. Glob. Change*, **13**, 425–436.

Hobbins, M. T., A. G. Dai, M. L. Roderick, and G. D. Farquhar, 2008: Revisiting the parameterization of potential evaporation as a driver of long-term water balance trends. *Geophys. Res. Lett.*, **35**, L12403, doi: 10.1029/2008GL033840.

Huang, R. H., Y. Liu, L. Wang, and L. Wang, 2012: Analyses of the causes of severe drought occurring in Southwest China from the fall of 2009 to the spring of 2010. *Chinese J. Atmos. Sci.*, **36**(3), 443–457. (in Chinese)

Hutchinson, M. F., 1998a: Interpolation of rainfall data with thin plate smoothing splines, Part I: Two dimensional smoothing of data with short range correlation. *Journal of Geographic Information and Decision Analysis*, **2**(2), 139–151.

Hutchinson, M. F., 1998b: Interpolation of rainfall data with thin plate smoothing splines Part II: Analysis of topographic dependence. *Journal of Geographic Information and Decision Analysis*, **2**(2), 152–167.

Li, Y. H., H. M. Xu, and D. Liu, 2009: Features of the extremely severe drought in the east of Southwest China and anomalies of atmospheric circulation in summer 2006. *Acta Meteorologica Sinica*, **25**(2), 122–132.

Maurer, E. P., and H. G. Hidalgo, 2008: Utility of daily vs. monthly large-scale climate data: An intercomparison of two statistical downscaling methods. *Hydrology and Earth System Sciences*, **12**, 551–563.

McEvoy, D. J., J. L. Huntington, J. T. Abatzoglou, and L. M. Edwards, 2012: An evaluation of multi-scalar drought indices in Nevada and eastern California. *Earth Interaction*, **16**, 1–18.

McKee, T. B., N. J. Doesken, and J. Kleist, 1993: The relationship of drought frequency and duration to time scales. Preprints, 8th *Conf. on Applied Climatology*, Anaheim, CA, Amer. Meteor. Soc., 179–184.

McKee, T. B., N. J. Doesken, and J. Kleist, 1995: Drought monitoring with multiple time scales. Preprints, 9th *Conf. on Applied Climatology*, Dallas, TX, Amer. Meteor. Soc., 233–236.

Moss, R. H., and Coauthors, 2010: The next generation of scenarios for climate change research and assessment. *Nature*, **463**, 747–756.

Nath, D., W. Chen, L. Wang, and Y. Ma, 2014: Planetary wave reflection and its impact on tropospheric cold weather over Asia during January 2008. *Adv. Atmos. Sci.*, **31**(4) doi: 10.1007/s00376-013-3195-8.

Palmer, W. C., 1965: Meteorological drought. U.S. Department of Commerce Research Paper 45, 58 pp.

Peng, J. B., Q. Y. Zhang, and C. Bueh, 2007: On the characteristics and possible causes of a severe drought and heat wave in the Sichuan-Chongqing region in 2006. *Climatic and Environmental Research*, **12**(3), 464–474. (in Chinese)

Qiu, J., 2010: China drought highlights future climate threats. *Nature*, **465**, 142–143.

Ren, G. Y., J. Guo, M. Z. Xu, Z. Y. Chu, L. Zhang, X. K. Zou, Q. X. Li, and X. N. Liu, 2005: Climate changes of China's mainland over the past half century. *Acta Meteorologica Sinica*, **63**(6), 942–956. (in Chinese)

Sun, L., F. M. Ren, Z. Y. Wang, Y. Y. Liu, Y. J. Liu, P. L. Wang, and D. Q. Wang, 2012: Analysis of climate anomaly and causation in August 2011. *Meteorological Monthly*, **38**(5), 615–622. (in Chinese)

Taylor, K. E., R. J. Stouffer, and G. A. Meehl, 2012: An overview of CMIP5 and the experiment design. *Bull. Amer. Meteor. Soc.*, **93**, 485–498.

Thornthwaite, C. W., 1948: An approach toward a rational classification of climate, *Geogr. Rev.*, **38**, 55–94.

Trewin, B. C., 2007: The role of climatological normals in a changing climate. World Climate Data and Monitoring Programme, WCDMP-No.61, WMO/TD No. 1377, 34 pp.

van der Schrier, G., P. D. Jones, and K. R. Briffa, 2011: The sensitivity of the PDSI to the Thornthwaite and Penman-Monteith parameterizations for potential evapotranspiration. *J. Geophys. Res.*, **116**, D03106, doi: 10.1029/2010JD015001.

Vicente-Serrano, S. M., S. Beguería, and J. I. López-Moreno, 2009: A multiscalar drought index sensitive to global warming: The Standardized Precipitation Evapotranspiration Index. *J. Climate*, **23**, 1696–1718, doi: 10.1175/2009JCLI2909.1.

Vicente-Serrano, S. M., S. Beguería, J. I. López-Moreno, M. Angulo, and A. El Kenawy, 2010: A new global 0.5° gridded dataset (1901–2006) of a multiscalar drought index: Comparison with current drought index datasets based on the Palmer Drought Severity Index. *J. Hydrometeor.*, **11**, 1033–1043, doi: 10.1175/2010JHM1224.1.

Vicente-Serrano, S. M., S. Beguería, and J. I. López-Moreno, 2011: Comment on "Characteristics and trends in various forms of the Palmer Drought Severity Index (PDSI) during 1900–2008" by Aiguo Dai. *J. Geophys. Res.*, **116**, D19112, doi: 10.1029/2011JD016410.

Vicente-Serrano, S. M., and Coauthors, 2012: Performance of drought indices for ecological, agricultural and hydrological applications. *Earth Interaction*, **16**, 1–27.

Wang, L., and W. Chen, 2012: Characteristics of multi-timescale variabilities of the drought over last 100 years in Southwest China. *Advances in Meteorological Science and Technology*, **2**(4), 21–26. (in Chinese)

Wang, L., and W. Chen, 2013: Application of bias correction and spatial disaggregation in removing model biases and downscaling over China. *Advances in Earth Science*, **28**(10), 1144–1153. (in Chinese)

Wang, L., and W. Chen, 2014: Applicability analysis of Standardized Precipitation Evapotranspiration Index in drought monitoring in China. *Plateau Meteorology*, **33**(2), 423–431. (in Chinese)

Wang, Z., F. Ren, L. Sun, Y. Liu, P. Wang, J. Tang, D. Wang, and D. Li, 2012: Analysis of climate anomaly and causation in summer 2011. *Meteorological Monthly*, **38**(4), 448–455. (in

Chinese)

Wei, K., W. Chen, and W. Zhou, 2011: Changes in the East Asian cold season since 2000. *Adv. Atmos. Sci.*, **28**(1), 69–79, doi: 10.1007/s00376-010-9232-y.

Wells, N., S. Goddard, and M. J. Hayes, 2004: A self-calibrating palmer drought severity index. *J. Climate*, **17**, 2335–2351.

Widmann, M., C. S. Bretherton, and E. P. Salathé, 2003: Statistical precipitation downscaling over the northwestern United States using numerically simulated precipitation as a predictor. *J. Climate*, **16**, 799–816.

Wilhite, D., 2006: Drought monitoring and early warning: Concepts, progress and future challenges. WMO-No. 1006, 24 pp.

Wood, A. W., E. P. Maurer, A. Kumar, and D. P. Lettenmaier, 2002: Long-range experimental hydrologic forecasting for the eastern United States. *J. Geophys. Res.*, **107**, doi: 10.1029/2001JD000659.

Wood, A. W., L. R. Leung, V. Sridhar, and D. P. Lettenmaier, 2004: Hydrologic implications of dynamical and statistical approaches to downscaling climate model outputs. *Climate Change*, **62**, 189–216, doi: 10.1023/B:CLIM.0000013685.99609.9e.

Xu, C. H., and Y. Xu, 2012: The projection of temperature and precipitation over China under RCP scenarios using a CMIP5 multi-model ensemble. *Atmos. Oceanic Sci. Lett.*, **5**(6), 527–533.

Yang, J., D. Gong, W. Wang, M. Hu, and R. Mao, 2012: Extreme drought event of 2009/2010 over southwestern China. *Meteor. Atmos. Phys.*, **115**, 173–184, doi: 10.1007/s00703-011-0172-6a.

Ye, T., P. Shi, J. Wang, L. Liu, Y. Fan, and J. Hu, 2012: China's drought disaster risk management: Perspective of severe droughts in 2009–2010. *International Journal of Disaster Risk Science*, **3**, 84–97, doi: 10.1007/s13753-012-0009-z.

Yuan, F., W. Chen, and W. Zhou, 2012: Analysis of the role played by circulation in the persistent precipitation over South China in June 2010. *Adv. Atmos. Sci.*, **29**(4), 769–781, doi: 10.1007/s00376-012-2018-7.

Zhang, J., L. Jiang, Z. Feng, and P. Li, 2012a: Detecting effects of the recent drought on vegetation in southwestern China. *Journal of Resources and Ecology*, **3**, 43–49.

Zhang, L., J. F. Xiao, J. Li, K. Wang, L. P. Lei and H. D. Guo, 2012b: The 2010 spring drought reduced primary productivity in southwestern China. *Environ. Res. Lett.*, **7**, 045706, doi: 10.1088/1748-9326/7/4/045706.

Zhang, M., J. He, B. Wang, S. Wang, S. Li, W. Liu, and X. Ma, 2013a: Extreme drought changes in Southwest China from 1960 to 2009. *Journal of Geographical Sciences*, **23**(1), 3–16, doi: 10.1007/s11442-013-0989-7.

Zhang, W. J., F. F. Jin, J. X. Zhao, L. Qi, and H. L. Ren, 2013b: The possible influence of a non-conventional El Niño on the severe autumn drought of 2009 in Southwest China. *J. Climate*, **26**, 8392–8405. doi: 10.1175/JCLI-D-12-00851.1.

Zhou, W., C. Li, and J. C. L. Chan, 2006: The interdecadal variations of the summer monsoon rainfall over South China. *Meteor. Atmos. Phys.*, **93**, 165–175, doi: 10.1007/s00703-006-0184-9.

Zhou, W., J. C. L. Chan, W. Chen, J. Ling, J. G. Pinto, and Y. Shao, 2009: Synoptic-scale controls of persistent low temperature and icy weather over southern China in January 2008. *Mon. Wea. Rev.*, **137**, 3978–3991, doi: 10.1175/2009MWR2952.1.